Validating the validation: the influence of liquid water distribution in clouds on the intercomparison of satellite and surface observations

N.A.J. Schutgens*, R.A. Roebeling
KNMI, the Netherlands

Correspondence address: Nick Schutgens, CCSR, University of Tokyo, 5-1-5 Kashiwanoha, Kashiwa, Chiba 277-8568, Japan
E-mail: schutgen@ccsr.u-tokyo.ac.jp

Abstract

The intercomparison of LWP retrievals from observations by a geostationary satellite imager (SEVIRI onboard MSG) and ground-based MW radiometer is examined in the context of cloud inhomogeneity. Although the influence of cloud inhomogeneity on satellite observations has received much attention, relatively little is known about its impact on validation studies.

This paper quantifies the various validation uncertainties due to cloud inhomogeneities and proposes an approach to minimize these uncertainties. The study is performed by simulating both satellite and ground-based observations for a set of high-resolution (100 m) cloud fields that are derived from 1 by 1 km^2 MODIS observations. Our technique for generating realistic high-resolution LWP fields preserves the information present in the original observations while creating extra LWP variation at smaller length-scales by considering clouds as simple fractals. To our knowledge, this is a new technique for creating high-resolution LWP fields.

Validation errors due to cloud inhomogeneity can be classified in two groups. The first group relates entirely to the retrieval process for satellite observations and includes the well-known plane parallel bias as well as mismatches between different channels. The second group relates to differences in the observed scene of both satellite and ground-based sensor. This includes systematic shifts in observed scene due to viewing conditions (parallax effect), offsets between satellite image and ground site as well as different field-of-views.

Of all the error contributions to the validation, the parallax effect easily tends to dominate for sites that are observed under large viewing angles (e.g. Northern Europe). We show that this error may be partly compensated by using information about cloud top heights and by spatial interpolation among an array of SEVIRI pixels to obtain the best estimate of the satellite retrieved LWP value over the ground site. Optimal intercomparison of satellite and ground-based observations is furthermore possible by matching the tracklength of the ground observations to the imager's pixel size in the wind direction.

One surprising conclusion is that the LWP errors due to the second group (scene differences) are significantly larger than those due to the first group (satellite retrieval), even after we have applied corrections. Equally surprising, smaller satellite pixels do not alleviate the problem but rather aggravate it, unless the parallax error is corrected. Calibration errors are not considered in the present study.

1. Introduction

Clouds are considered an important but poorly understood aspect of the climate system (Kristjansson et al. 2000; Potter and Cess 2004). Their presence modulates the radiative balance (Slingo 1990) and hence the energy available to drive atmospheric dynamics, the hydrological cycle and global warming. As cloud radiative properties on a macro scale (cloud albedo and cloud lifetime) are expected to depend on cloud microphysics (Twomey 1977; Albrecht 1989), detailed observations of clouds are a prerequisite for a better understanding of the climate system.

Polar-orbiting satellites allow global coverage on a time-scale of a few days, while geostationary satellites allow coverage of a significant part of the Earth on timescales of 10's of minutes. Satellite observations are thus very interesting from the point-of-view of cloud studies. Minnis et al. (1992) combined surface observations with geostationary GOES visual and thermal infra-red radiances to determine COT (cloud optical thickness) and cloud top height. Nakajima and King (1990) were the first to develop an algorithm to derive COT and effective particle size from combined satellite radiance observations at 0.75 and 2.16 μm. This technique was later applied to AVHRR observations (Nakajima and Nakajima 1995; Kuji et al. 2000). The dual-view capacity of ATSR-2 was employed by Evans and Haigh (1995) to retrieve COT and effective particle size. Currently, MODIS (Moderate Resolution Imaging Spectroradiometer) flown on the Acqua and Terra platforms are providing detailed information on cloud microphysics (King et al. 1997; Platnick et al. 2003).

The imhomogeneous nature of water cloud macro- and microphysical horizontal structure has received much attention. For a wide variety of cloud types, satellite imagery shows that cloud properties (perimeter, area, radiances) exhibit a power law in their spectral distribution (Cahalan and Joseph 1989; Cahalan and Snider 1989; Barker and Davies 1992; Lovejoy et al. 1993). The observed break in this power-law at small scales (~ 300 m) was shown to be due to radiative effects and is not an intrinsic property (Davis et al. 1997; Oreopoulos et al. 2000). The same power law has been observed in in-situ LWC (liquid water content) observations (Davis et al. 1999; Gerber et al. 2001; Siebert et al. 2006) as well as ground-based radiometer observations (see previous papers). Therefor, the radiance variability is commonly understood as resulting from LWC being passively advected in a turbulent medium.

The previously mentioned retrieval techniques all assume homogeneous clouds, so it is no surprise that a lot of research has been devoted to this obviously flawed assumption. When discussing the effect of cloud inhomogeneity on cloud retrievals it is useful to distinguish between errors due to the plane parallel assumption and due to shadowing and illumination. The plane parallel assumption refers to the internal variation of COT (or LWP, liquid water path) and is usually dominant at larger length scales (several km and above). The shadowing/illumination error refers to the interaction between radiation and variations in cloud-tops and is typically dominant at smaller length scales (1 km and below). Cahalan et al. (1994) and Barker and Davies (1992) studied the effect of the plane-parallel bias on either albedo or radiative fluxes and found they were reduced compared to those for homogeneous clouds. On the other hand, Iwabuchi and Hayasaka (2002) showed that at small scales, shadowing/illumnination can cause both under- or overestimation depending on the scattering geometry (see also Loeb et al. (1998)). Marshak et al. (2006); Zinner and Mayer (2006); Kato et al. (2006), using detailed 3D radiative transfer calculations for high resolution cloud fields, found that in general LWP was underestimated while effective size was overestimated.

For observational studies of the impact on cloud inhomogeneity, see e.g. Várnai and Mar-

shak (2002), who studied illumination/shadowing in the case of MODIS observations, or Dim et al. (2007), who compared observations from a geostationary satellite (GMS-5/SVISSR) to those from a polar orbiting satellite (Terra-MODIS). Both groups of authors concluded that LWP can be either under- or overestimated, depending whether one looks at an illuminated or shadowy cloudside.

For theoretical studies of the radiative effects of cloud variability, different cloud models have been employed. Early studies used (bounded) cascade models to generate horizontally variable LWP fields (Schertzer and Lovejoy 1987; Cahalan 1994; Marshak et al. 1994). Later studies were conducted for LES (large eddy simulations) clouds (Marshak et al. 2006; Zinner and Mayer 2006; Kato et al. 2006). Techniques for artificially creating cloud fields based on observations have also been developed (Venema et al. 2006) (see Hogan and Kew (2005) for creating cirrus clouds).

Validation of satellite observations with ground observations has been performed by various authors (see e.g. previously mentioned papers). But the effect of inhomogeneity on such validation effort has received little attention. In this paper, we will study the effect of horizontal LWP and particle size inhomogeneity on the intercomparison of satellite with ground-based observations. In particular, we will concern ourselves with LWP observations by the SEVIRI imager onboard the geostationary MSG satellite and ground-based MW radiometers in Northern-Europe. The analysis is performed by, first, creating realistic high resolution (100 m) LWP fields (derived from MODIS observations) and, next, simulating satellite imager and ground-based MW radiometer LWP retrievals. This study is therefor theoretical and allows definition of a truth LWP. Consequently, we can analyse the different error contributions to the validation. One group of errors are entirely due to the assumption of homogeneous clouds in the satellite retrieval. Another set of errors are due to the actual comparison of data from sensors with different fields-of-view (FOV).

Water clouds also exhibit vertical inhomogeneity, often displaying (quasi-) adiabatic profiles (Brenguier et al. 2000; Pawlowska et al. 2000; Schüller et al. 2003). Clearly, this will impact comparison of LWP measurements by two different sensors, especially as one sees the top of the cloud (satellite) and the other the bottom (ground site). However, the focus of this paper is on horizontal variability and vertical inhomogeneity will be ignored.

In Sect. 3, we describe the selection of MODIS cloudfields (with a resolution of 1 km) that will be used in Sect. 4 to create realistic high resolution (100 m) LWP fields. In Sect. 5, we describe how we simulate the LWP validation and consider in detail the various error contributions. This section also considers possible improvements in the validation procedure. Finally, Sect. 6 contains a summary with conclusions.

2. SEVIRI sensor

Meteosat Second Generation (MSG) is a new series of European geostationary satellites that is operated by EUMETSAT. In August 2002 the first MSG satellite (METEOSAT-8) was launched succesfully, while in December 2005 the second MSG satellite (METEOSAT-9) was launched. The MSG is a spinning stabilized satellite that is positioned at an altitude of about 36 000 km above the equator at 3.4^oW for METEOSAT-8 and 0.0^o for METEOSAT-9.

The SEVIRI instrumment scans the complete disk of the Earth 4 times per hour and operates 12 channels simultaneously. There are 3 solar channels (0.6, 0.8 and 1.6 μm), 8 infrared channels (3.9, 6.2, 7.3, 8.7, 9.7, 10.8, 12.0 and 13.4 μm) and one high resolution braodband

visible channel (0.3–0.7 μm).The nadir spatial resolution of SEVIRI is 1 by 1 km^2 for the high-resolution channel and 3 by 3 km^2 forthe okther channels. By sensing in narrow and numerous wavelength bands, it is possible to identify specific cloud and surface properties as well as obtain information on the composition and thermodynamic charactersitics of the atmosphere. Six of SEVIRI's channels are about similar to those of the AVHRR instrument onboard the NOAA and METOP polar orbiting satelllites.

3. The MODIS data

Our purpose in this section is to show how we selected the contiguous MODIS cloud fields that will later be used to create artificial but realistic high-resolution LWP fields. To briefly describe this technique, we propose to use observed LWP variability over a 10 by 10 km^2 contiguous cloudfield to represent LWP variability at 100 m, after appropriate scaling. At the very least, this requires that we have two datasets, one of contiguous l by l km^2 cloudfields that serve as the main cloud scene, and one of contiguous 10 by 10 km^2 fields that are used to create variability at 100 m scales. In principle, both datasets may contain the same clouds, but the paucacity of useful observations over land meant that we were forced to base our 10 by 10 km^2 fields on observations over ocean.

We used MODIS collection 5 cloud product from both the Terra and Acqua platforms for the period of August 2006 upto and including July 2007, over Northern Europe and the North Atlantic. Searching for contiguous cloudfields over land, it became obvious that $l = 25$ km was an optimal choice of field size. Larger fields rapidly become infrequent in the MODIS dataset, while smaller fields simply do not have the spatial coverage required for our analysis (see Sect. 5). All in all, we found 604 contiguous 25 by 25 km^2 cloudfields, that will later serve as scenes.

In addition, we found 1329 contiguous 30 by 30 km^2 cloudfields over ocean which will be used to provide the required 10 by 10 km^2 fields. Searching in the MODIS dataset for contiguous 10 by 10 km^2 fields does not increase the number of found fields, while the 30 by 30 km^2 fields have a certain advantages over their smaller brethren that will become apparent later.

Of course, the MODIS dataset contains many more (contiguous) cloudfields than we found for this period and location. But we applied other criteria as well, to arrive at the most reliable spatial distributions of LWP possible. Those criteria will now be briefly discussed. Relevant information always came from the MODIS MOD06 level 2 cloud product.

First, we looked for 5 by 5 km^2 fields which were tagged confidently as water clouds (based on infra-red observations) and were observed under optimal viewing conditions. We required solar zenith angle $\theta_0 < 60^o$ and scattering angle $100^o \leq \Theta \leq 180^o$ as Loeb and Coakley (1998) showed that inverting satellite observed radiances into cloud properties is most reliable for such scattering geometries. Viewing angles were limited to $\theta \leq 10^o$.

Second, we looked at the individual 1 by 1 km^2 MODIS pixels and required that they were confidently cloudy with no cirrus or heavy aerosol present. To allow for the best possible retrievals, observations over sun-glint and/or ice or snow were discarded. Again, cloud phase was checked (the MODIS cloud phase product for 1 and 5 km is based on different algorithms, R. Frey 2007, personal communication).

Finally, the confidence (as assessed by the MODIS team) for the cloud optical thickness, LWP and effective particle size were all required to be very good.

All l by l km^2 cloudfields thus found where required to be spatially separated (center-to-center) by at least a distance of $l\sqrt{2}$. This prevented overlap of cloudfields and allowed us to view the cloudfields as independent samples of spatial LWP distributions.

A random subset of the selected 25 by 25 km^2 clouds over land and 30 by 30 km^2 clouds over ocean was visually inspected. It turned out that some LWP fields over ocean showed a high degree of local clustering that could be indicative of drizzling or even raining clouds in our sample. After demanding that no field has individual pixels with a LWP > 500 g/m^2 or $r_{\text{eff}} > 15\,\mu$m, scenes with such strong clustering were severely reduced.

Looking at the sample averages for the main cloud parameters, we see the following. The observations are equally split among the Terra and Acqua platforms, and they yield similar cloud optical thickness, LWP and effective particle size. There is a marked land/ocean contrast, which can be either real or due to the difference in sampling. Cloud optical thickness (24.1 vs 15.4) and LWP (125 vs 98 g/m^2) are higher for the clouds over land than over ocean, presumably because our criterium of contiguity implies only very thick clouds make the grade over land. Effective particle size is larger over the ocean (9.7 μm) than over land (8.1 μm), as has been shown to be the case in many studies. The variability (half theLWP interquantile range between 16% and 84% of the distribution divided by median LWP) is a bit larger for clouds over land than over ocean (0.36 vs 0.30). Overall, the variability in effective particle size (0.10) is much smaller than that of LWP (0.30-0.36).

It is interesting to take a closer look at the LWP variability found in the cloudfields over land. From Fig. 1 we see that no cloudfield is truly homogeneous, allthough some show little variation. The distribution is skewed to larger values, implying that strongly inhomogeneous fields will occur more often than just the sample mean and standard deviation would suggest. Fig. 2 shows the standard deviation of the difference between LWP in neighbouring 1 by 1 km^2 pixels as a function of distance. Obviously, strong correlations exists within our cloudfields within the first 5 km of a pixel, but at larger distances LWP seems uncorrelated. Notice also the isotropic character of our sample. Finally, from Fig. 3 it is clear that the variability in effective particle size is not nearly as pronounced as the variability in LWP.

We stress that the sample of contiguous cloudfields thus obtained is not a statistically representative selection of water clouds. In particular, thin clouds will be under represented and broken clouds are, by virtue of contiguency, not present. However, we feel that the present sample shows realistic spatial distributions of LWPṠince this is a comparitive study of retrieval errors, this should be sufficient.

4. Constructing high resolution fields

In this section we will discuss the algorithm used to create high resolution LWP fields from MODIS observations. High-resolution, in our case, means that the new LWP field will have a sampling distance of 100 m (instead of 1 km), but this does not reflect a limitation of the technique.

If we take the common wisdom that clouds are fractal structures to be true, a simple algorithm for creating high resolution LWP fields readily presents itself. A fractal, after all, is a 'rough or fragmented geometric shape that can be subdivided into parts, each of which is (at least approximately) a reduced-sized copy of the whole' (Mandelbrot, 1982). This so-called self-similarity implies that the LWP structure over, say, 10 km is equally representative of the LWP structure at 1 km or 100 m. As a matter of fact, many simple fractals are created by re-

producing a basic structure at smaller and smaller spatial scales, see e.g. the Koch snowflake or the Sierpinski sieve.

In our case, we start with a single 30 by 30 km^2 cloud field (observed over ocean) and calculate the interquartile range Δ' of the LWP difference between 1 by 1 km^2 pixels that are separated by 10 km. This represents the variability at a spatial scale of 10 km. Next, we select the four 10 by 10 km^2 fields that are located in the corners of this 30 by 30 km^2 field (there will be little correlation among these fields, see the discussion of Fig. 2). Take one such field LWP$'_{i,j}$ (where $i, j = 1 \ldots 10$ are the pixel coordinates) and calculate its mean value $|\text{LWP}'|$. A 'normalized' LWP distribution can then be defined as

$$G_{i,j} = \left(\text{LWP}'_{i,j} - |\text{LWP}'|\right) / \Delta'. \tag{1}$$

After repeating this procedure for all 30 by 30 km^2 fields, we are left with $1329 \times 4 = 5316$ fields that can be taken to represent LWP structure at any (!) spatial scale (assuming the fractal character holds at that scale).

Next we take a 25 by 25 km^2 cloudfield over land (see Fig. 4) and calculate the interquartile range Δ of the LWP difference between neighbouring 1 by 1 km^2 pixels. We then sub-divide each 1 by 1 km^2 pixel into 100 by 100 m^2 sub-pixels. If the original pixel has observed water content of value LWP, then the sub-pixels will be assigned values

$$\text{LWP}_{i,j} = \text{LWP} + \Delta * G_{i,j} \quad i, j = 1 \ldots 10. \tag{2}$$

Notice that the total LWP of the original pixel remains unchanged as the sum of $G_{i,j}$ is zero. In essence, we use a 10 by 10 km^2 field ($G_{i,j}$) to represent variability at 100 m after appropriately scaling the variability in the field. Note that the original variability at 10 km is scaled to match the variability at 1 km.

What remains to be decided is how to choose a particular field $G_{i,j}$ to fill-in a 1 by 1 km^2 pixel. A first approach would be to select a random field $G_{i,j}$ for each 1 by 1 km^2 pixel. The resulting cloud scene might look like the one shown in Fig 5. Although the power-law is clearly present and extends to shorter spatial scales, the LWP field shows large and arbitary jumps across the boundaries of the original 1 by 1 km^2 pixels.

A better approach would be to match the sub-pixels $G_{i,j}$ in neighbouring pixels, in such a way that the average jump *across* the pixel boundary matches the variation *among* the sub-pixels. If our database of G-fields is large enough, this should be possible. For instance, one might start by randomly selecting G for staggered 1 by 1 km^2 pixels, like the black fields on a chess or checkers board. Next, one searches for the appropriate G for the white fields on our chess board, making sure that the variation across the pixel boundary matches the variation within the pixel. Here, variation implies the interquartile range of the difference in LWP between neighbouring 100 by 100 m^2 sub-pixels (or a similar statistical measure). Experience, however, shows that matching the G's in the white chess board fields to their 3 or 4 neighbouring fields leaves large residual errors (jumps) unless one has a very large dataset to choose G's from.

Instead we use a different approach, starting with a random G-field for the top-left pixel. The G-field for the second pixel from the left on the top line is then matched on to this. And then the G-field for the third pixel from the left is matched to the LWP field just created. And so on. At the end of the top-line, move down one line and repeat the process. In this way G-fields only have to match at most 2 neighbouring fields, greatly reducing the size of the dataset required. An example of a resulting cloud field can be seen in Fig. 6. The method preserves the

power-law fairly well. The slight curve present in the graph is very typical of all fields created in the manner described in this paragraph. The chess board tiling technique, probably since it allows more randomness, shows a straighter line, like the one in Fig. 5.

On a 2.66 GHz MacIntel, a single 25 by 25 km cloud field may be filled in like this in a bit more than 4 min. Of course, much depends on the size of the collection of G fields, which in our case numbered $5316 \times 4 = 21264$ (four orientations per 10 by 10 km^2 field). The implementation was made in IDL.

Creating LWP fields at higher resolution than 100 m is very simple. Either one repeats the present algorithm at smaller scales, i.e. one now fills in the 100 by 100 m^2 sub-pixels (arriving at a final sampling distance of 10 m) or one uses larger size G-fields, e.g. the full 30 by 30 km^2 (arriving at a final sampling distance of 33.3 m).

We point out that the final LWP fields are identical to the original MODIS retrieved LWP fields on a 1 km scale. In addition, the fine structure they exhibit up to scales of 100 m conforms with the oft-observed power-law.

5. Modelling the SEVIRI LWP validation

In this section, we discuss how cloud inhomogeneity affects the validation of SEVIRI LWP with ground-based MW radiometer data. We present an approach to model the validation accuracy and discuss the applicability of the approximations inherent in our method. Finally, we present simulated error statistics for the validation of SEVIRI LWP with MW -radiometer values.

Cloud inhomogeneity affects LWP validation because both sensors (satellite and ground-based radiometer) see different parts of the same cloudfield at different times. This is a direct consequence of the different spatial and temporal sampling strategies employed by the sensors. The satellite samples (almost instantaneously) a large 2-dimensional view of the cloud from above, while the MW radiometer samples a narrow swath from below, as the clouds drift over the observations site.

Imagine a cloudfield as discussed in the previous section. Such a field represents the LWP distribution at a single moment near a ground site (see Fig 7). The FOV of SEVIRI is represented by elongated diamonds (due to the SEVIRI view angle of $\theta \sim 60^o$, as is the case for Cabauw, Chilbolton and Palaisseau, see Table 1, Illingworth et al. (2007)). The solid diamond is the official SEVIRI pixel closest to the ground site. Supposedly, this pixel will compare most favourably with LWP at the ground site. Unfortunately, the 60^0 view angle also implies that the observed cloud, located at some altitude above the surface, really has a different geo-location than the actual SEVIRI pixel, which is thought to be located at the Earth's surface. Clouds on the Northern hemisphere are actually to the south of the pixel geo-location to which they are attributed. This parallax effect is explained in the inset of Fig. 7. The arrow represents the view direction of SEVIRI and explains why the FOV is shifted to the south of the pixel.

Since this cloudfield is an instantaneous LWP distribution, we need further assumptions to represent the MW radiometer observations. If, for the duration of an observation by the ground site, this cloudfield is merely advected without internal evolution (frozen turbulence theorem), then the MW radiometer observation may be represented by a narrow track. Note that the track will differ with windspeed, wind direction (NW or SE in the figure) and cloud altitude. Although SEVIRI time movies show the frozen turbulence assumption to be a rather poor approximation on time-scales of 15 min., it allows us to develop a simple frame-work for

our intercomparison of SEVIRI and MW radiometer observations. In actuality, the LWP does not have to be advected passively by the flow. As long as the flow does not modify the statistics of the LWP distribution (so-called stationarity), our conceptual model should remain valid. See also Feijt and Jonker (2000) who found remarkable agreement in spatial variation of satellite observations and temporal variation in ground obsevations.

Clearly, we will not concern ourselves with the divergence of observations caused by the different view-points (from above or below). This is mainly a retrieval issue and involves detailed studies of radiative transfer. More-over, it exists independently of cloud inhomogeneity. We will also not concern ourselves with the temporal evolution of cloudfields, but simply note that this would cause an additional random error contribution in some of our error budgets.

Before analyzing in-depth the different error contributions, we introduce the concept of the ideal SEVIRI pixel. This is a virtual SEVIRI pixel, with the same point spread function as an actual SEVIRI pixels, but centered at a particular ground site.

Also, we will present error statistics not through the usual standard deviation, but through inter-quantile ranges. This is necessary because of the strong non-Gaussian nature of the error statistics. The stochastic parameters we will discuss are Q_{50} (the median, i.e. the bias), $\Delta Q_{68} = Q_{84.2} - Q_{15.8}$ (which would be double the standard deviation for a Gaussian error distribution) and $\Delta Q_{95} = Q_{97.75} - Q_{2.25}$ (four times the standard deviation for a Gaussian error distribution). Sometimes, the word variation will be used to indicate ΔQ_{68} of a distribution.

a. Radiative effect on MSG retrievals

In this subsection, we will look at the effect that inhomogenity has on the LWP retrievals by SEVIRI. By looking for observed radiances at 0.66 and 1.6 μm in a look-up table (LUT), COT, LWP and effective particle size may be determined. However, such LUT's are usually calculated for homogeneous clouds, and SEVIRI is no exception in this respect.

Cloud inhomogeneity adds considerable complexity to radiative transfer and the inversion of radiances to cloud physical properties. The errors it causes in retrievals are generally classified as either a plane-parallel bias or shadowing/illumination error. Typically, shadowing/illumination errors dominate at short spatial scales ($\sim$ 1 km) while the plane-parallel bias dominates at larger scales. It thus stands to reason to assume that the retrieval of LWP for SEVIRI is most affected by the plane-parallel bias.

Under the independent column approximation, the LUT's allow us to calculate radiances at 100 m resolution. After suitably averaging these radiances over the SEVIRI FOV, we obtain simulated SEVIRI observations of radiance at 0.66 and 1.6 μm. Now the LUT's may again be used, this time to retrieve LWP for the SEVIRI FOV. The discrepancy between actual and retrieved LWP in this FOV is the plane-parallel bias. Note that the independent column approximation is valid as long as the overall error due to radiative effects is dominated by this plane-parallel bias. Note also that the lower variability of effective particle size as compared to LWP implies that LWP-inhomogeneity is the dominant factor. As a matter of fact, using an $r_{\rm eff}$ varying over the FOV or an average value causes negligible differences.

It is well known that the plane-parallel bias causes an underestimation of COT, which in turn causes an underestimation of LWP. In this respect, our results are no different (see Fig. 8). For our cloudfields, the underestimation of COT is often associated with an overestimation of $r_{\rm eff}$, somewhat balancing the errors in LWP. Thus, average underestimation of COT is 50 % larger than that for LWP, while average *over* estimation for $r_{\rm eff}$ is 20 % smaller than the LWP *under* estimation. This overestimation is in agreement with previous studies (Marshak et al. 2006;

Zinner and Mayer 2006; Kato et al. 2006).

Up to now, we have implicity assumed that the FOV's for the 0.6 and 1.6 μm channel are identical. As a matter of fact, they are not. Different sensors are used to observe radiances at these wavelengths, and the alignment of the observations is hampered by thermal stresses in the instrument. The difference in the 0.6 and 1.6 μm FOV's can be modelled as a random offset (Gaussian) with a standard deviation of ~ 320 m in both east-west and north-south directions EUMETSAT team (2006, p. 33). For homogeneous clouds, such an offset (we call it the NIR wobble) would be harmless, but in the case of inhomogeneity it will lead to additional LWP errors. These errors are the differences in *retrieved* LWP for observations made with or without NIR wobble and are shown in Fig. 9. These errors are symetrically distributed around zero and smaller than the plane-parallel bias. Due to the random nature of the FOV offset, there is no correlation between this error and the plan-parallel bias.

As for the effect of scattering geometry on these results, there seems to be none. We have performed the same analysis for three different scattering geometries ($\theta_o = 45.7^o, 29.8^o, 53.2^o$, $\phi - \phi_o = 72^o, 4^o, 78^o$) as might occur for SEVIRI throughout a day (at 9, 12 and 16 hour GMT) but found no differences that might not be explained as statistical noise. The underlying reaon for this, of course, is that the LUT's themselves do not change drastically with viable viewing geometry.

Finally, we consider the effect that the size of the NIR wobble has on the LWP error. Figure 10 shows the errors due to this wobble only and due to wobble and plane parallel bias combined. The latter is of course larger and moreover has a negative bias (not shown). As the wobble increases, the difference in the two errors decreases, since the plane parallel bias remains unchanged. Also shown is the actual error due to the NIR wobble for SEVIRI.

b. Error due to parallax effect

As shown in Fig. 7, the cloud actually observed differs from the cloud present at the location of the pixel, due to the 60^o viewing angle (parallax effect). For cloud-top heights of 2 km, this yields a south-ward shift of 3.46 km, hardly negligible compared the SEVIRI FOV size. The associated error is defined as the difference between actual LWP in the FOV and in the pixel.

Fig. 11 shows a histogram of cloud top heights for Chilbolton, for situations when only water clouds were present. If we randomly assign an observed cloud top height to each of our cloudfields (assuming constant height over the whole field), the errors due to the parallax effect can be simulated. These errors are symmetrically distributed around zero (even though the southward shift itself has a bias of 2980 m, $\tan 60^o$ times the median of cloud top height).

Of course, this result depends strongly on the cloudtop height distribution. In Fig. 12, we examine the influence of a constant shift in cloudtop heights. I.e., for a shift of 0 m, the error shown corresponds to the error given in the previous paragraph. For non-zero shifts, we changed the cloudtop distribution of Fig. 11 accordingly and then recalculated errors. The different lines are for different cloudtop height distributions (for Chilbolton, Palaisseau, and Chilbolton again with different criteria to select water clouds). So if clouds are on average 500 m higher, associated errors will increase by 10 g/m^2.

c. Error due to pixel offset from the ideal pixel

The offical SEVIRI pixel is usually offset from the imaginary, ideal pixel whose centre coincides with the ground site (see Fig. 7). This offset consists of a constant offset depending

on the location of the ground site (see Table 1) and of a random offset due to improper image navigation. The error due to the constant offset is estimated to be $\Delta Q_{68} = 21.1, 28.6$ and 17.2 g/m^2 for respectively Cabauw, Chilbolton and Palaiseau. The error due to improper image navigation is ~ 4 g/m^2 fo all sites.

In Fig. 10, we study the influence of the size of the image navigation error on LWP errors. For simplicity, we assumed that the random offset EUMETSAT team (2006, p. 32), we call it the VIS wobble, is similar in North-South and East-West directions at SSP. We see that for SEVIRI , image navigation has a relatively small contribution to the overall error budget. But this error increases more rapidly with increasing wobble, implying that for a wobble 2 or 3 times larger, it would be more important than the error due to radiative effects.

d. Total error budget for SEVIRI

We are now in a position to assess the total LWP error budget with respect to the ideal pixel due to cloud inhomogeneity. Most error sources have distinctly different physical reasons and therefor uncorrelated errors. The one exception are the errors due to parallax and pixel offset. These errors can either amplify or mitigate each other, depending on whether the pixel is located to the north or south of the site. The parallax effect, of course, always shifts the FOV southward (at least on the northern hemisphere). A summary of the error budget is found in Table 2 .

Certain errors, those due to LUT's for homogenous clouds or due to wobbles, should be identical for each site. The observed discrepancies result from statistical noise. Since pixel offsets are different for each site, we locate each site at a different position within our 25 by 25 km cloudfields to accomodate all FOV's (official pixel, ideal pixel, observed FOV, MW radiometer tracks). Consequently error statistics will vary slightly.

Table 2 shows that the errors due to parallax and pixel offset are the dominating contributions. Note, however, that they may partly cancel each other. For Chilbolton, located to the south of the pixel, there is a weak anti-correlation ($r = -0.49$) between the errors due to parallax and site offset. This reduces overall LWP errors somewhat. Cabauw, on the other hand, is located mainly to the west of the pixel and only 155.8 m south of the SEVIRI pixel and the anti-correlation between parallax and site off-set is much less ($r = -0.18$). Finally, for Palaiseau, the offset error is smallest. Even though the geographical distance of the site to the pixel is similar to Cabauw's, the relative distance (ratioed to the pixel's size) is twice as small. Since Palaisseau has the largest N-S offset associated errors correlate positively ($r = 0.57$) with the parallax errors. Consequently, overall LWP error is largest for Palaisseau.

We point out the extreme non-Gaussian nature of the error statistics, with ΔQ_{95} being typically three times as large as ΔQ_{68}.

Finally, it is interesting to consider the effect a smaller SEVIRI pixel would have on these error budgets. Here we consider those pixels halved in both NS and EW directions, while at the same time their sampling distance is halved. Also, as part of the improved resolution, we assume that the wobbles have been reduced by 50 %. Error budgets are shown in Table 3 and show some surprising results. First, understandably, errors due to retrieval and wobble are reduced (note that for a smaller pixel, retrieval errors may have more contribution from shadowing/illumination, an effect we do not model). Errors due to parallax are significantly larger as the smaller pixel size offers less chance of cancelling errors. The offset error depends of course, strongly on the exact sampling positions of the pixels (we assume the original sampling plus additional pixels halfway). The (anti) correlations between parallax and offset errors increases and in general overall errors are significantly increased.

The preceding analysis should not make one forget that the LWP error budget for SEVIRI observations is purely due to the LUT's for homogenous clouds and the NIR/ pixel wobble. We already see here, what will become more obvious in the next section, that validation actually introduces larger errors than the retrieval itself.

e. Spatial interpolation of MSG LWP fields

In this subsection, we investigate how effective one can perform spatial interpolation on a grid of SEVIRI pixels. We ask ourselves the question: 'with what accuracy can we obtain the LWP of a virtual pixel from a spatial array of real SEVIRI pixels. This will be useful to know when comparing SEVIRI observations to MW radiometer observations later on, when the virtual pixel will be imagined centered on a ground site.

Spatial interpolation in two dimensions may be accomplished by many different schemes. In practice we limit ourselves to a few simple schemes, which are as follows. The first scheme simply uses LWP at the nearest real SEVIRI pixel. In the bilinear scheme, the LWP values of the four nearest SEVIRI pixels are bilinearly interpolated to obtain the value at the virtual pixel. In the inverse4 scheme LWP at the four nearest pixels are averaged with weights determined by the inverse of their distance to the virtual pixels. Finally, we also considered a scheme where a Gaussian weighting over the four nearest pixels of the virtual pixel is calculated. This scheme requires a choice for a typical scale-length (Gaussian 'spread'); experiments show that for $L = 0.75$ interpolation errors are minimal. From our sample of 604 cloudfields we may easily determine both the actual LWP in the virtual pixel and the interpolates. As independent variables in the interpolation, we used pixel indices rather than physical distance.

Error statistics are shown in Table 4 for the three ground sites considered in this study: Cabauw, Chilbolton and Pallaiseau. Of the schemes considered, bilinear interpolation and Gaussian averaging seem to be the most accurate, with the bilinear interpolation slightly better (but this maybe due to our choice of ground sites or statistical noise). The biases (Q_{50}) due to these schemes are generally less than 1 g/m^2.

f. Validation of SEVIRI with MW radiometer observations

Using the frozen turbulence assumption, we can easily model the LWP observations by the MW radiometer and compare these to the SEVIRI observations. If we assume that each MW radiometer observation is based on integration over a fixed time-interval, then different windspeeds translate into tracks of various length. First, we will compare MW radiometer observations to those for the ideal SEVIRI pixel whose center coincides with a ground site. Also, error contributions to SEVIRI LWP due to radiative effects will ,for now, be ignored.

In Fig. 13, the validation error as a function of track length and wind direction is shown (there are negligible, positive biases, that we will not discuss). Two things are readily apparent: errors depend on wind-direction and become minimal for an optimal tracklength. Unsurprising, validation for N-S winds at the optimal tracklength is more succesful, as the mean distance of the track to the pixel's edges is smaller. The optimal tracklength depends slightly on wind-direction; it is ~ 7.5 km for E-W and ~ 9 km for N-S direction, which agrees with the pixel being larger along the N-S direction. For other winds there is a gradual variation with directions. Away from the optimal tracklength, validation errors for al wind-directions is quite similar. Overall, errors show a strong non-Gaussian distribution with Q_{95} typically 2.5 to 3 times larger than Q_{68}.

Next, we compare MW radiometer LWP for Cabauw to that observed in the actual SEVIRI FOV. This analysis takes into account the errors due to radiative effects, parralax and pixel offset as well. Not surprising, errors are now significantly larger, as is shown in Fig. 14. There is much less difference between the wind-directions and tracklengths. Errors are distributed in a strong non-Gaussian fashion $\Delta Q_{95}/\Delta Q_{68} =\sim 3$. Smallest errors that one can expect are given in Table 5 and 6.

The validation errors shown in Fig. 14 can be explained from the 1) the errors (ϵ_1) between the ideal pixel and the MW radiometer observations as presented at the beginning of this section; 2) the errors (ϵ_2) between the actual SEVIRI FOV and the ideal pixel as discussed in the preceding sections. This is especially true for radiometer observations made at optimal tracklengths when the correlations between ϵ_1 and ϵ_2 are minimal ($|r| < 0.1$. The sum of the squared errors $\sqrt{\epsilon_1^2 + \epsilon_2^2}$ yields very good agreement with Table 5, allowing for statistical noise. However, for shorter tracklengths a weak negative correlation exists between ϵ_1 and ϵ_2 ($-0.3 \leq r \leq -0.2$), while for long tracklengths a weak positive correlation ($0.0 \leq r \leq 0.4$) exists. In the latter case, this correlation depends strongly on wind direction.

The absence of a significant correlation between ϵ_1 and ϵ_2 for the optimal tracklengths suggests that the concept of the ideal SEVIRI pixel is useful.

The effect of a reduced SEVIRI pixel is shown in Fig. 15. The top panel shows validation errors for the ideal pixel. Due to the smaller pixel size, optimal tracklengths are shorter and smallest errors are lower than for the current SEVIRI pixel size (compare to Fig. 13). The bottom panel shows validation errors for the observed pixel. These errors are now larger than for the current SEVIRI pixel as the smaller pixel is more sensitive to LWP inhomogeneity (compare to Fig. 13).

Finally, we consider the improvement in LWP correspondence, when corrections for the parallax error and offset error are introduced. The pixel offset error may be corrected by spatial interpolation in between neighbouring SEVIRI pixels, since the location of the ground site with respect to the SEVIRI pixel array is known. The accuracy of various interpolation schemes was investigated in the previous subsection. If we know cloudtop height, or at least a climatological average, we may similarly correct for the parallax error. Results for the Cabauw station are shown in Fig. 16. In the top panel, it is assumed we have accurate cloudtop height for each observed cloud. This allows us to reduce minimal LWP errors to 23.8 g/m^2 (N-S winds) and 29.2 g/m^2 (E-W winds). Note that the latter error is, within statistical noise, similar to the error for the ideal pixel, while the first is significantly larger. In the bottom panel, the median of the cloud top distribution was used to correct for the parallax error. The ΔQ_{68} errors are hardly affected (21.3 and 31.9 g/m^2), but the ΔQ_{95} errors for E-W wind are significantly higher. Using a climatological average of cloudtop height results in error distribution that are more strongly non-Gaussian and wider. Finally, we see that correcting for pixel offset and parallax in the case of reduced pixels yields smaller errors. Note, however, that the improvement is rather small ($\sim 20\%$).

6. Summary and conclusion

In this paper, we have provided a detailed error budget for the validation of satellite observations of inhomogeneous clouds with ground observations. In particular, we studied the agreement between LWP retrievals by the SEVIRI imager onboard the geostationary satellite MSG and ground-based MW radiometer in Northern-Europe. Since both sensors employ differ-

ent sampling strategies, they effectively see different clouds although there will be an overlap. If clouds were homogeneous, this would not be an issue but cloud inhomogeneity strongly affects the validation effort. We do not consider the effect of incorrect calibration on the validation, nor that of horizontal photon transport (shadowing/illumination). We argue that this is a valid approximation for the large SEVIRI pixels (3 by 3 km^2 at nadir).

Our methodology is based on realistic but artificial 2-dimensional high-resolution LWP fields, derived from MODIS observations. A new technique for filling in LWP variability at length scales below 1 km was developed, that is consistent with current knowledge of cloud variability. The resulting 2-dimensional LWP distributions still exhibit the original LWP distribution as observed by MODIS at length-scales of 1 km and larger. Some 604 fields of 25 by 25 km^2 and a 100 m resolution are used to study the impact of differences in the aforementioned sampling strategies. Consequentially, simulated LWP observations may be compared amongst themselves and with the known truth for an detailed error budget. In particular, we are able to separate the various error contributions inherent to validation: radiative effects in the retrieval by the satellite LWP (due to LUT's developed for homogeneous clouds and a VIS/NIR channel FOV mismatch), incorrect image navigation and systematic offsets between satellite and ground site location, shifts in geo-location of satellite-observed clouds due to the parallax effect, and the difference in satellite and radiometer FOV.

We draw several conclusions from this study. First, error distributions are highly non-Gaussian implying that standard deviations are not the proper statistic to describe LWP errors. In particular, error distributions are wider than the standard deviation would suggest, leading to underestimates of the error if this statistic is used. Instead, we use quantile ranges like ΔQ_{68} and ΔQ_{95}. Secondly, among the different error sources that we considered, the errors inherent to the satellite retrieval of LWP over inhomogeneous clouds (e.g. LUTs developed for homogeneous clouds, mismatch of the IFOV of different satellite channels) is smaller than the errors due comparison of satellite and ground-based radiometer derived LWP. In other words, validation of satellite LWP observations introduces larger errors than the retrieval process itself. Of course, our study does not include satellite calibration errors (estimated at 20 %, Govaerts and Clerici (2004)), but then again, neither do we include retrieval errors for the MW radiometer (estimated at 30 g/m^2, Löhnert and Crewell (2003))

Among the errors due to comparison of satellite and ground-based derived LWP, those due to the parallax effect are clearly dominating for a geostationary satellite and ground-stations in Northern Europe (latitude $\sim 50^o$). To some extent, these errors maybe compensated if cloud top altitudes are known and a sufficiently extended cloud field exists that allows for spatial interpolation of LWP. But even if the center of the observed cloud coincides with the ground-station, different FOV's of the satellite and radiometer allow for larger errors than the retrieval from satellite observations by itself. However, it is possible to minimize those errors by matching the integration time for the radiometer and prevalent windspeeds (and directions) to the satellite pixel size. Not surprisingly, integrated tracklengths should resemble the pixel size. For ground-station that are observed under a high viewing angle, distortion of the pixel implies that final error statistics and optimal tracklengths are different for East-West winds than for Nouth-South winds.

Surprisingly, validation results do not improve when smaller satellite pixels are used, but rather deteriorate further, unless care is taken to correct for the errors due to parallax and pixel offset. The reason for this is that larger pixel sizes partly compensate for the parallax error due to overlap of the geo-location of the pixel and its shifted FOV. If, however, parallax and pixel

offset errors are corrected for, smaller satellite pixels allow tighter error budgets. A pixel that is half the size of the SEVIRI pixel (i.e. only 25% of its area) would yield an improvement in LWP validation (decrease in total error budget) of not more than $\sim 20\%$.

1) *

Acknowledgments. The authors gratefully acknowledge stimulating discussions with Dr A. Feijt, H. Deneke and W. Greuell. This study was started while the first author was employed at KNMI, and financed through the SYNTHESIS project.

References

Albrecht, B., 1989: Aerosols, cloud microphysics and fractional cloudiness. *Science*, **245**, 1227 – 1230.

Barker, H. and J. Davies, 1992: Cumulus cloud radiative proerties and the characteristics of stellite radiance wavenumber spectra. *Rem. Sens. Environ.*, **42**, 51 – 64.

Brenguier, J.-L., H. Pawlowska, L. Schüler, R. Preusker, J. Fischer, and Y. Fouquart, 2000: Radiative properties of boundary layer clouds: droplet effective radius versus number concentration. *J. Atmos. Sci.*, **57**, 803 – 821.

Cahalan, R., 1994: Bounded cascade clouds: albedo and effective thickness. *Nonlin. Proc. Geophys.*, **1**, 156 – 167.

Cahalan, R. and J. Joseph, 1989: Fractal statistics of cloud fields. *Mon. Weather Rev.*, **117**, 261 – 272.

Cahalan, R., W. Ridgway, W. Wiscombe, S. Gollmer, and Harshvardhan, 1994: Independent pixel and Monte Carlo estimates of stratocumulus albedo. *J. Atmos. Sc.*, **51**, 3776 – 3790.

Cahalan, R. and J. Snider, 1989: Marine stratocumulus structure. *Rem. Sens. Environ.*, **28**, 95 – 107.

Davis, A., A. Marshak, R. Cahalan, and W. Wiscombe, 1997: The Landsat scale break in stratocumulus as a three-dimensional radiative transfer effect: implications for cloud remote sensing. *J. Atmos. Sci.*, **54**, 241 – 259.

Davis, A., A. Marshak, H. Gerber, and W. Wiscombe, 1999: Horizontal structure of marine boundary layer clouds from centimeters to kilometers scale. *J. Geophys. Res.*, **104**, 6123 – 6143.

Dim, J., T. Takamura, I. Okada, T. Nakajima, and H. Takenaka, 2007: Influence of inhomogeneous cloud fields on optical proerties retrieved from satellite observations. *J. Geophys. Res.*, **112**, doi:10.1029/2006JD007891.

EUMETSAT team, 2006: *MSG level 1.5 Image Data Format Description*. EUMETSAT, eum/msg/icd/105 edition.

Evans, S. and J. Haigh, 1995: The retrieval of total optical depth and effective droplet radius of clouds from solar reflection measurements using the along track scanning radiometer-2 (ATSR-2). *Geophys. Res. Letters*, **22**, 695 – 698.

Feijt, A. and H. Jonker, 2000: Comparison of scaling parameters from spatial and temporal distributions of cloud properties. *J. Geophys. Res.*, **105**, 29 089 – 29 097.

Gerber, H., J. Jensen, A. Davis, A. Marshak, and W. Wiscombe, 2001: Spectral density of cloud liquid water content at high frequencies. *J. Atmos. Sc.*, **58**, 497 – 503.

Govaerts, Y. and M. Clerici, 2004: Evaluation of radiative transfer simulations over bright desert calivration sites. *IEEE Trans. on Geoscience and Remote Sensing*, **42**, 176 – 187.

Hogan, R. and S. Kew, 2005: A 3D stochastic cloud model for investigating the radiative properties of inhomogeneous cirrus clouds. *Q. J. R. Meteo. Soc.*, **131**, 2585 – 2608.

Illingworth, A. J., R. Hogan, E. Connor, D. Bouniol, M. Brooks, J. Delanoë, D. Donovan, N. Gaussiat, J. Goddard, M. Haeffelin, H. Klein Baltink, O. Krasnov, J. Pelon, J.-M. Piriou, A. Protat, H. Russchenberg, A. Seifert, A. Tompkins, G.-J. van Zadelhoff, F. Vinit, U. Willén, D. Wilson, and C. Wrench, 2007: CLOUDNET continuous evaluation of cloud profiles in seven operational models using groundbased observations. *Bull. Amer. Meteor. Soc.*, **88**, 883 – 898.

Iwabuchi, H. and T. Hayasaka, 2002: Effects of cloud inhomogeneity on the optical thickness retrieved from moderate-resolution satellite data. *J. Atmos. Sci.*, **59**, 2227 – 2242.

Kato, S., L. Hinkelman, and A. Cheng, 2006: Estimate of satellite-derived cloud optical thickness and effective radius errors and their effect on computed domain-averaged irradiances. *J. Geophys. Res.*, **111**, doi:10.1029/2005JD006668.

King, M., S. Tasy, S. Platnick, M. Wang, and K. Liou, 1997: Cloud retrieval algorithms for MODIS: optical thickness, effective particle radius and thermodynamic phase. MODIS algorithm theoretical basis document MOD-05, MOD-06, NASA.

Kristjansson, J., J. Edwards, and D. Mitchell, 2000: Impact of a new scheme for optical properties of ice crystals on climates of two gcms. *J. Geophys. Res.*, **105**, 10063–10079.

Kuji, M., T. Hayasaka, N. Kikuchi, T. Nakajima, and M. Tanaka, 2000: The retrieval of effective particle radius and liquid water path of low-level marine clouds from NOAA AVHRR data. *J. Appl. Meteor.*, **39**, 999 –1016.

Loeb, N. and J. Coakley, 1998: Inference of marine stratus cloud optical depths from satellite measurements: does 1D theory apply? *J. Clim.*, **11**, 215 – 233.

Loeb, N., T. Várnai, and D. Winker, 1998: Influence of subpixel-scale cloud-top structure on reflectances from overcast stratiform cloud layers. *J. Atmos. Sci.*, **55**, 2960 – 2973.

Löhnert, U. and S. Crewell, 2003: Accuracy of cloud liquid water path from ground-based microwave radiometry. Part i: Dependency on cloud model statistics. *Radio Sci. /*, **38**, 6 – 11.

Lovejoy, S., D. Schertzer, P. Silas, Y. Tessier, and D. Lavallée, 1993: The unified scaling model of atmospheric dynamics and systematic analysis of scale invariance in cloud radiances. *Ann. Geophys.*, **11**, 119 – 127.

Marshak, A., A. Davis, R. Cahalan, and W. Wiscombe, 1994: Bounded cascade models as nonstationary multifractals. *Phys. Rev. E*, **49**, 55 – 69.

Marshak, A., S. Platnick, T. Várnai, G. Wen, and R. Cahalan, 2006: Impact of three-dimensional radiative effects on satellite retrievals of cloud droplet sizes. *J. Geophys. Res.*, **111**, doi:10.1029/2005JD006686.

Minnis, P., P. Heck, D. Young, C. Fairall, and J. Snider, 1992: Stratocumulus cloud properties derived from simultaneous satellite and island-based instrumentation during FIRE. *J. Appl. Meteor.*, **31**, 317 – 339.

Nakajima, T. and M. King, 1990: Determination of the optical thickness and effective particle radius of clouds from reflected solar radiation measurements. 1. Theory. *J. Atmos. Sci.*, **47**, 1878 – 1893.

Nakajima, T. and T. Nakajima, 1995: Wide-area determination of cloud microphysical properties from NOAA AVHRR measurements for FIRE and ASTEX regions. *J. Atmos. Sci.*, **52**, 4043 – 4059.

Oreopoulos, L., A. Marshak, R. Cahalan, and G. Wen, 2000: Cloud three-dimensional effects evidenced in landsat spatial power spectra and autocorrelation functions. *J. Geophys. Res.*, **105**, 14 777 – 14 788.

Pawlowska, H., J. Brenguier, and F. Burnet, 2000: Microphysical properties of stratocumulus clouds. *Atmos. Res.*, **55**, 15 – 33.

Platnick, S., M. King, S. Ackerman, W. Menzel, B. Baum, R. J.C. and R. Frey, 2003: The MODIS cloud products: algorithms and examples from Terra. *IEEE Trans. Geosci. & Rem. Sens.*, **41**, 459 – 473.

Potter, G. and R. Cess, 2004: Testing the impact of clouds on the radiation budgets of 19 atmospheric general circulation models. *J. Geophys. Res.*, **109**, doi:10.1029/2003JD004018.

Schertzer, D. and S. Lovejoy, 1987: Physical modelling and analysis of rain and clouds by anisotropic scaling multiplicative processes. *J. Geophys. Res.*, **92**, 9693 – 9714.

Schüller, L., J. Brenguier, and H. Pawlowska, 2003: Retrieval of microphysical, geometrical and radiative properties of marine stratocumulus from remote sensing. *J. Geophys. Res.*, **108**, doi:10.1029/2003JD003902.

Siebert, H., K. Lehmann, and M. Wendisch, 2006: Observations of small-scale turbulence and energy dissipation rates in the cloud boundary layer. *J. Atmos. Sci.*, **63**, 1451 – 1466.

Slingo, A., 1990: Sensitivity of the earth's radiation budget to changes in low clouds. *Nature*, **343**, 49–51.

Twomey, S., 1977: The influence of pollution on the shortwave albedo of clouds. *J. Atmos. Sci.*, **34**, 1149 – 1152.

Várnai, T. and A. Marshak, 2002: Observations of three-dimensional radiative effects that influence MODIS cloud optical thickness retrievals. *J. Atmos. Sci.*, **59**, 1607 – 1618.

Venema, V., S. Meyer, S. Garcia, A. Kniffka, C. Simmer, S. Crewell, U. Löhnert, T. Trautmann, and A. Macke, 2006: Tellus. *58A*, **1**, 104 – 120.

Zinner, T. and B. Mayer, 2006: Remote sensing of stratocumulus clouds: uncertainties and biases due to inhomogeneity. *J. Geophys. Res.*, **111**, doi:10.1029/2005jd006955.

List of Figures

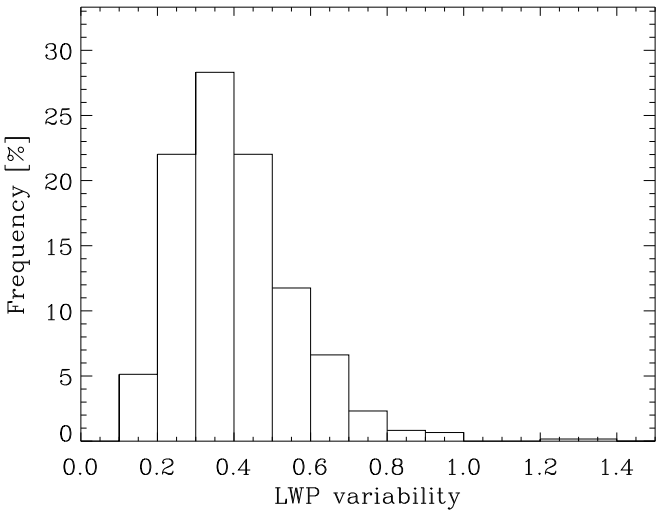

FIG. 1. Histogram of LWP variability (defined in the text) for our sample of 604 25 by 25 km^2cloudfields over land.

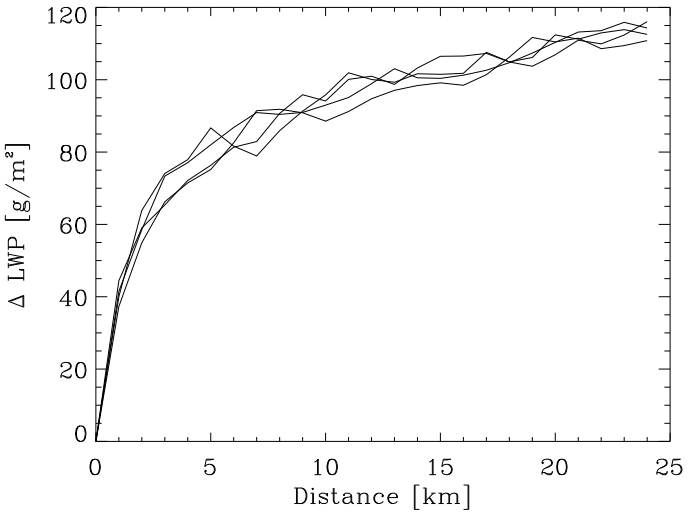

FIG. 2. Difference in LWP (within the same cloudfield), as a function of distance, from one of the corners of a 25 by 25 km^2 cloudfield. Different lines belong to different corners and different directions (up, down, left or right) in the field. Standard deviation calculated for our sample of 604 25 by 25 km^2 fields over land.

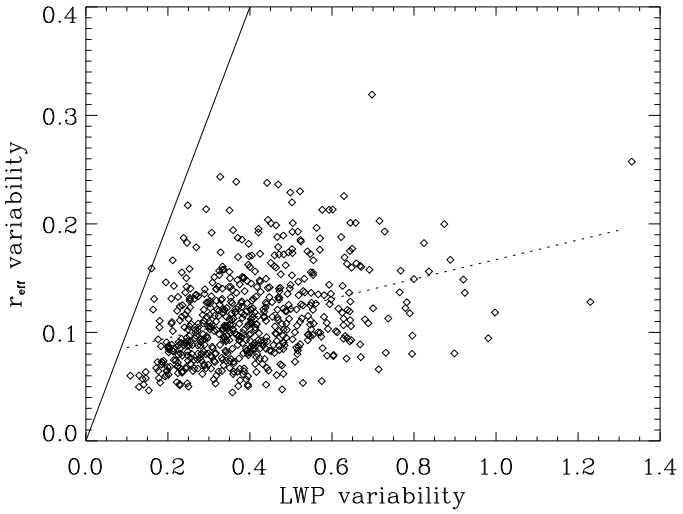

FIG. 3. Variability in LWP vs. variability in $r_{\rm eff}$, for our sample of 604 25 by 25 km^2 fields over land. The solid line represents at 1:1 correspondence, the dashed line is a linear fit to the observations.

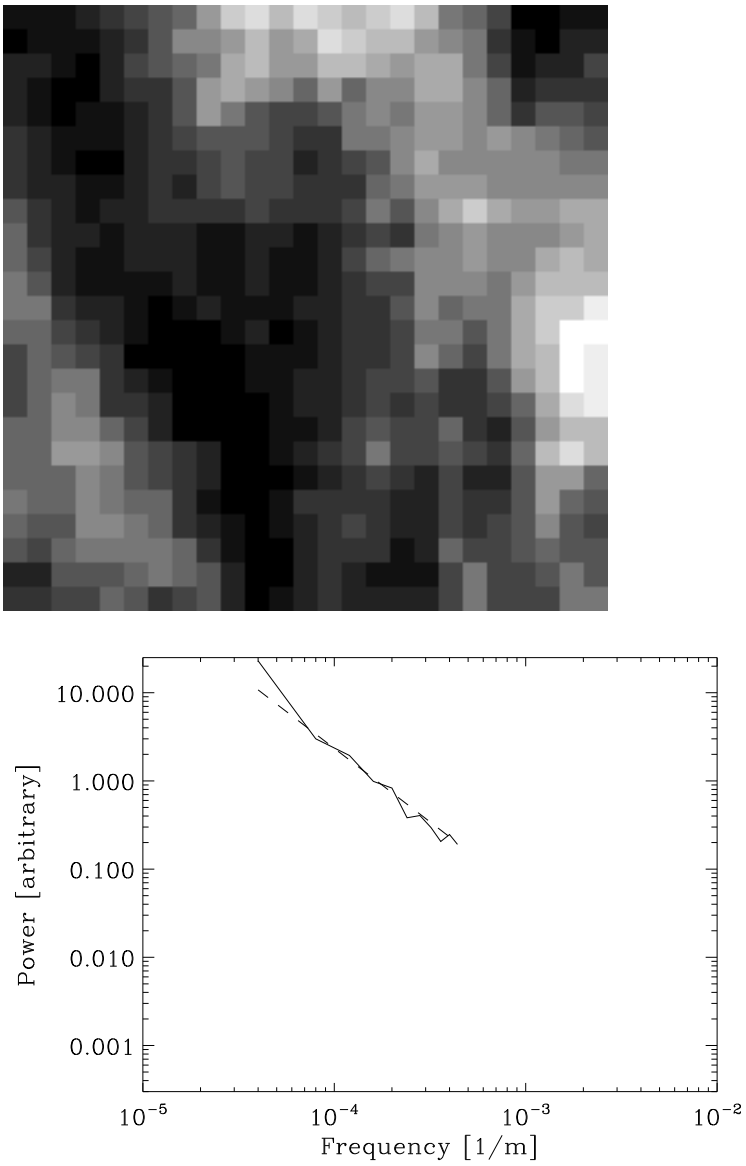

FIG. 4. Example of an original 25 by 25 km^2 distribution of LWP as observed by MODIS. Also shown is the associated power spectrum. The dashed line is a fit to a -5/3 power law.

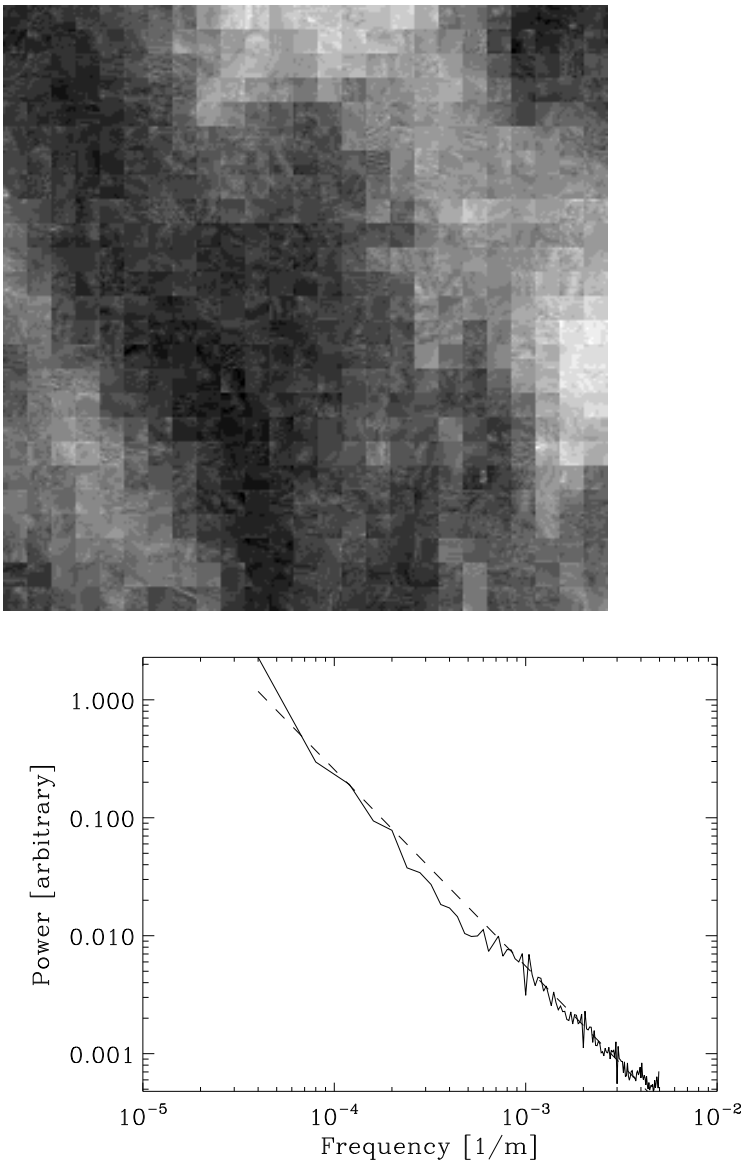

FIG. 5. The same cloud scene as in Fig. 4. Each MODIS 1 by 1 km^2 pixel is filled in with a random choice for LWP distribution, drawn from a dataset of 10 by 10 km^2 observations. Also shown is the associated power spectrum. The dashed line is a fit to a -5/3 power law.

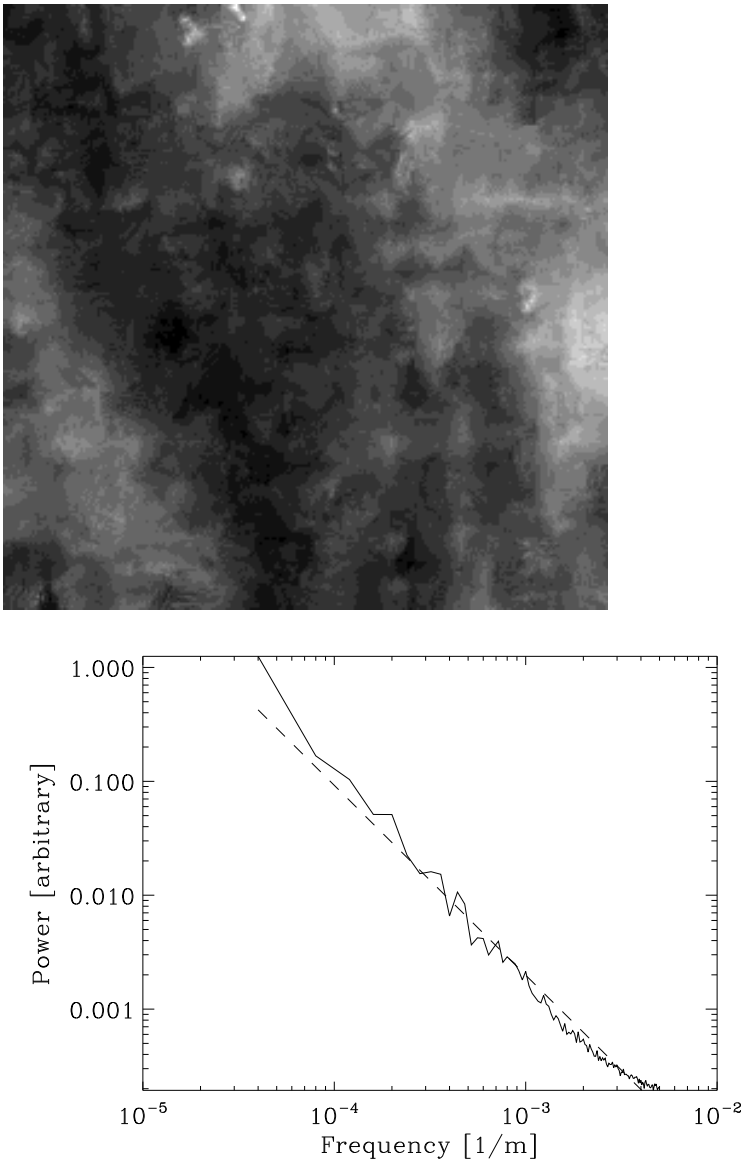

FIG. 6. The same cloud scene as in Fig. 4. Each MODIS 1 by 1 km^2 pixel is filled in by an LWP distribution (from a dataset of 10 by 10 km^2 observations) that best matches its neighbouring pixels. Also shown is the associated power spectrum. The dashed line is a fit to a -5/3 power law.

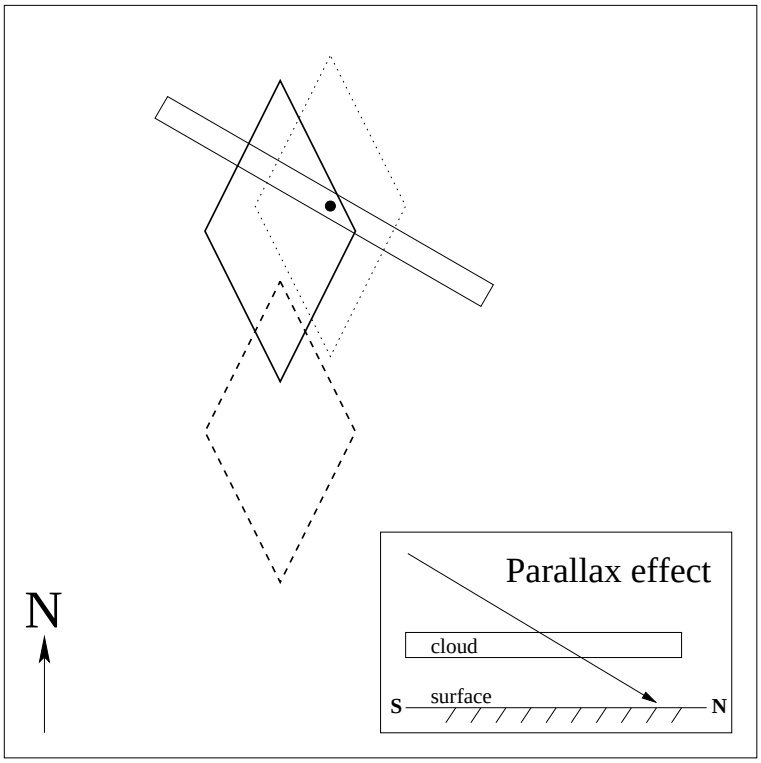

FIG. 7. A conceptual image of the sampling strategies for SEVIRI and MW -radiometer. The solid diamond is the actual SEVIRI pixel closest to the ground site (dot). Due to the parallax effect, the cloud actually observed, however, is located to the south (dashed diamond). The dotted diamond centered on the ground site is the so-called ideal SEVIRI pixel. The track running NW-SE represents the MW -radiometer FOV.

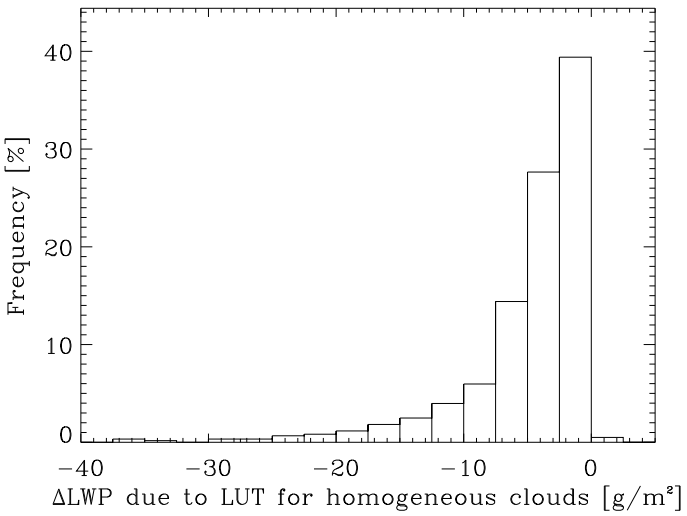

FIG. 8. The plane-parallel bias in retrieved LWP due to the use of LUT's for homogeneous clouds ($\theta_0 = 29.8^o, \theta = 59.1^o, \phi - \phi_0 = 4^o$).

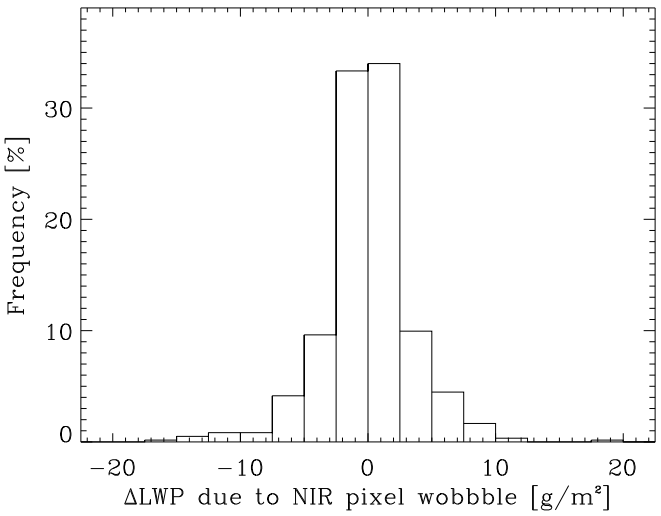

FIG. 9. LWP error due the mismatch in 0.6 and 1.6 μm FOV's and the use of LUT's for homogeneous clouds ($\theta_0 = 29.8^o, \theta = 59.1^o, \phi - \phi_0 = 4^o$).

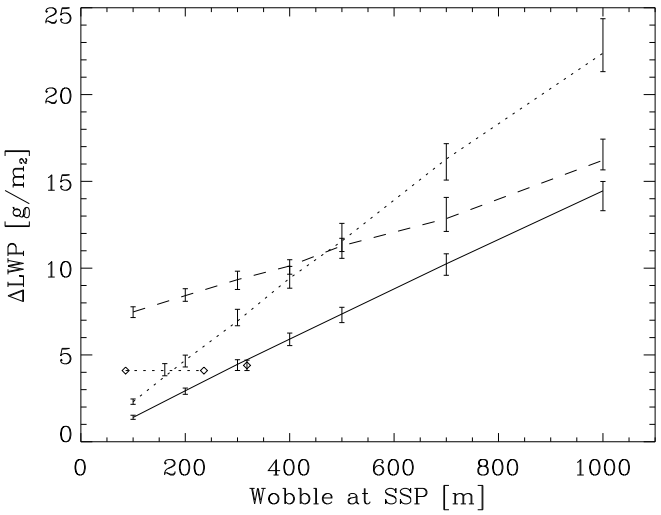

FIG. 10. LWP errors due to either the NIR or VIS pixel wobble for varying wobble distances. LWP errors due to the NIR wobble only (solid line) and NIR wobble plus plane parallel bias (dashed line) are shown as function of the standard deviation of the wobble. The dotted line is the error due to the VIS wobble (see Sect. 5). Also shown are errors for actual SEVIRI pixel wobbles (diamonds).

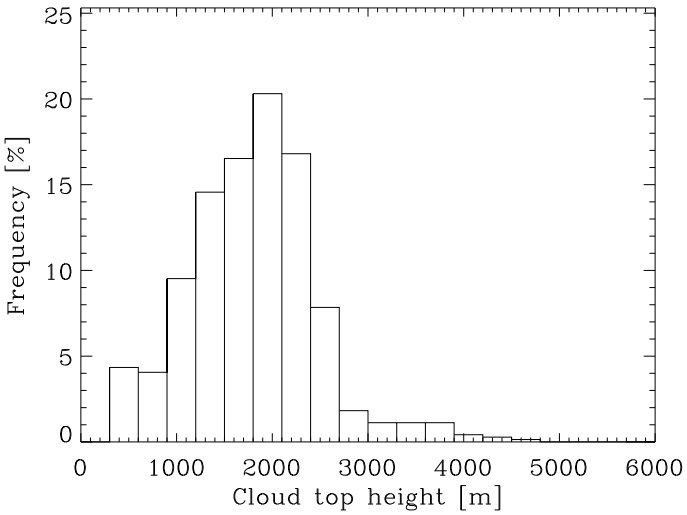

FIG. 11. Cloud top heights observed over Chilbolton for May to September 2004, obtained from the CloudNet project. Cloud top heights were derived from radar measurements.

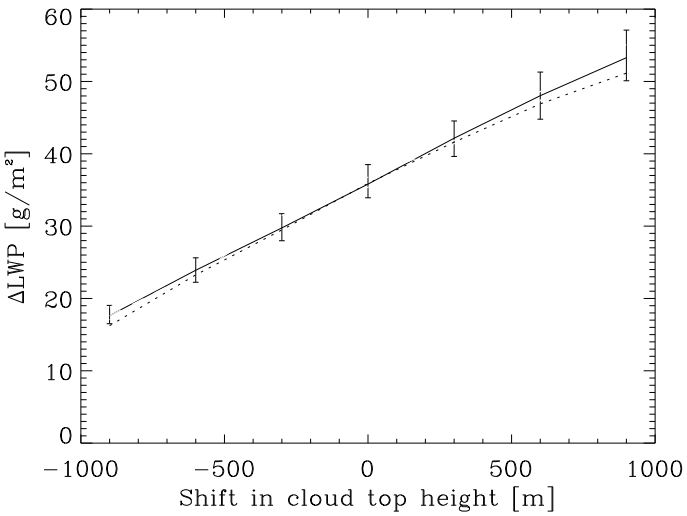

FIG. 12. LWP error due to the parallax effect. Solid line is for the cloud top height distribution at Chilbolton, dotted line is at Palaisseau.

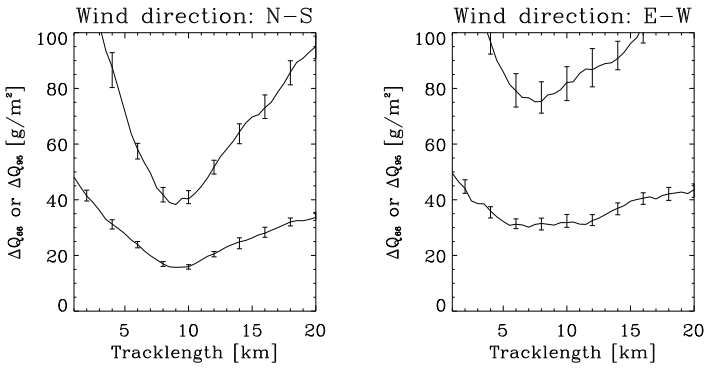

FIG. 13. Validation errors in LWP for the ideal pixel as a function of tracklength (MW radiometer integration time) and wind-direction. Errors due to statistical noise are indicated with error bars.

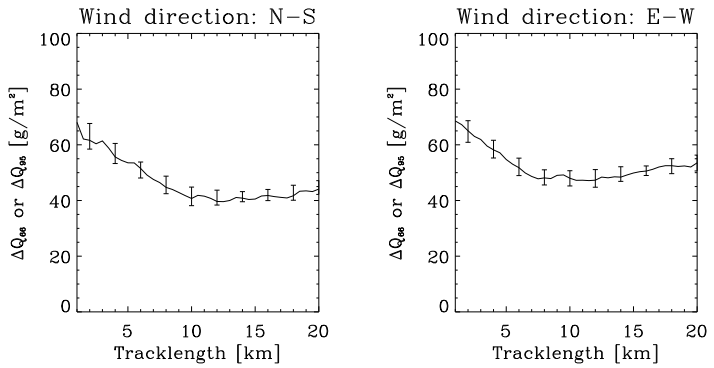

FIG. 14. Validation errors in LWP for the actual SEVIRI pixel nearest to Cabauw as a function of tracklength (MW radiometer integration time) and wind-direction. Errors due to statistical noise are indicated with error bars. Note that the Q_{95} errors are larger than 100 g/m^2.

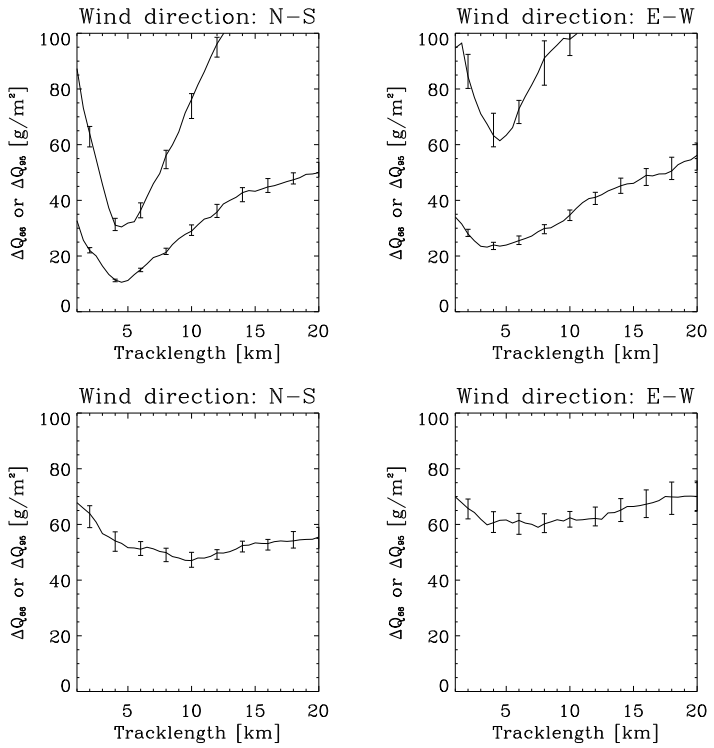

FIG. 15. Validation errors in LWP for the reduced size pixel as a function of tracklength (MW radiometer integration time) and wind-direction. Top panels for the ideal pixel and bottom panels for the Cabauw FOV. Errors due to statistical noise are indicated with error bars. Note that the Q_{95} errors are larger than 100 g/m^2 in the lower panels.

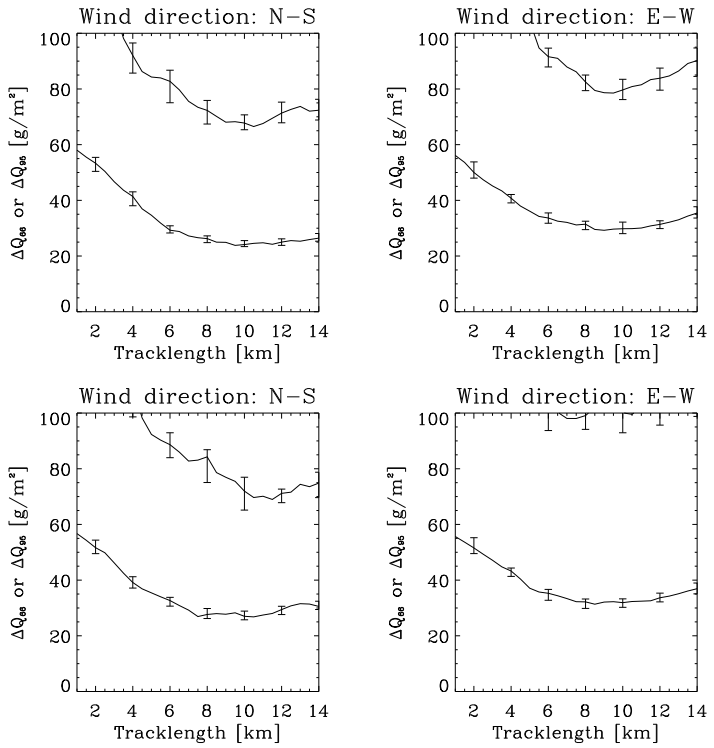

FIG. 16. Validation errors in LWP for the Cabauw pixel as a function of tracklength (MW radiometer integration time) and wind-direction, if parallax and pixel offset are accounted for. Top panels i.c. the exact cloud top height is known and bottom panels i.c. a climatological cloud top height is used. Errors due to statistical noise are indicated with error bars.

List of Tables

TABLE 1. Geo-location of the ground sites used in this study.

	location [^{o}]		pixel offset [km]	
	lon	lat	EW	NS
Cabauw	4.93	51.97	1.4	0.2
Chilbolton	-1.44	51.14	1.6	1.1
Palaisseau	2.21	48.71	-0.4	-1.2

TABLE 2. Error budget for LWP determined for SEVIRI observations with respect to the ideal pixel.

	Cabauw		Chilbolton		Palaisseau	
	ΔQ_{68}	ΔQ_{95}	ΔQ_{68}	ΔQ_{95}	ΔQ_{68}	ΔQ_{95}
LUT homog	7.8	22.2	7.2	21.9	7.1	21.2
NIR wobble	4.1	15.0	3.7	15.0	3.7	15.4
parallax	32.3	115.3	35.3	111.3	31.7	111.9
site	21.1	66.5	28.6	86.0	17.2	46.5
VIS wobble	4.4	18.6	4.1	19.0	4.3	15.4
total	38.6	126.7	33.6	102.4	46.1	138.0

TABLE 3. Error budget for lwp determined from a sensor with twice the resolution of SEVIRI.

	Cabauw		Chilbolton		Palaisseau	
	ΔQ_{68}	ΔQ_{95}	ΔQ_{68}	ΔQ_{95}	ΔQ_{68}	ΔQ_{95}
LUT homog	4.8	13.2	4.6	13.3	5.3	16.2
NIR wobble	3.6	13.2	3.7	12.6	3.8	13.2
parallax	49.6	177.6	52.7	170.8	52.6	181.5
site	6.7	21.0	25.3	66.8	29.0	78.6
VIS wobble	3.7	15.4	3.6	16.0	3.7	14.9
total	46.8	175.1	37.6	138.3	73.6	219.5

TABLE 4. Error budget for spatial interpolation of MSG LWP fields.

	Cabauw	Chilbolton	Palaiseau
nearest	22.0	24.8	17.3
bilinear	9.0	13.6	11.1
inverse4	21.1	18.5	14.7
Gauss4, $L = 0.75$	9.3	13.2	11.9

TABLE 5. Minimal total error budget for comparison of SEVIRI and radiometer LWP, for North-South winds.

	pixel location			
	ideal	Cabauw	Chilbolton	Palaiseau
no correction	15.4	39.6	38.9	45.2
climate cloud top		26.8	25.2	23.7
actual cloud top		23.8	22.6	19.5
actual cloud top, reduced pixel		19.2	18.7	17.3

TABLE 6. Minimal total error budget for comparison of SEVIRI and radiometer LWP, for East-West winds.

	pixel location			
	ideal	Cabauw	Chilbolton	Palaiseau
no correction	30.3	47.1	44.0	58.0
climate cloud top		31.3	34.8	33.8
actual cloud top		29.2	31.4	31.7
actual cloud top, reduced pixel		25.6	30.6	30.1